Available online at www.sciencedirect.com
ScienceDirect
Trans. Nonferrous Met. Soc. China 34(2024) 1710−1720
Transactions of Nonferrous Metals Society of China
www.tnmsc.cn

Effect of gas flow rate and nozzle diameter on bubble size and shape distributions in bubble column

Hong-jie YAN[1], He-yang ZHANG[1], Liu LIU[1], Thomas ZIEGENHEIN[2], Ping ZHOU[1]

1. School of Energy Science and Engineering, Central South University, Changsha 410083, China;
2. TIV Consultancy, 7th Pl Road 1312, 85281 Tempe, Arizona, United States

Received 22 November 2022; accepted 12 October 2023

Abstract: The influence of gas flow rates and nozzle diameters on bubble size and aspect ratio distributions was studied using high-speed photography with an image processing algorithm. Results reveal bimodal probability density distributions (PDD) of bubble diameter under all nozzle diameters, with one peak near 1.5−2 mm and the another in the larger bubble range. Increasing gas flow rates from 0.1 to 0.2 L/min leads to a higher probability density of large bubbles, indicating prevalent bubble coalescence. As the gas flow rate rises to 1.2 L/min, the peak shifts to smaller bubble diameters, and the bubble breakage becomes dominant. For 1−2 mm bubbles, shape is less influenced by gas flow rates, while 3−9 mm bubbles exhibit aspect ratio PDD peaks at an aspect ratio (E) of 0.5 across all gas flow rates. The Iguchi and Chihara model can better predict the variation of bubble departure diameter with increasing gas flow rates.
Key words: bubble size distribution; bubble diameter; bubble aspect ratio; gas flow rate; nozzle diameter; bubble column

1 Introduction

Gas−liquid two-phase flows find widespread applications across industries, including chemical, energy, and biological processes [1−3]. The behavior of bubbles within these flows plays a pivotal role in determining the efficiency of mass, momentum, and energy transfer between the gas and liquid phases. In industrial equipment such as vertical pipes and bubble columns, understanding the dynamics of bubble size and shape distributions is essential for optimizing process performance and system design.

The bubble size distribution (BSD) is one of the most critical parameters influencing bubble column hydrodynamics. Accurate BSD data are indispensable for precise computational fluid dynamics (CFD) modeling in bubble columns, with the Euler−Euler method relying heavily on precise interfacial closure. While traditional methods commonly employ the sphere-volume equivalent diameter as a fundamental parameter for BSD characterization in numerical simulations, the population balance model demands a clear comprehension of bubble size distribution under different conditions to make reasonable assumptions and applications [4]. Therefore, investigating complex BSD under varying flow conditions is of paramount importance, as it will provide intricate insights into experimental phenomena, subsequently offering detailed information for numerical simulations [5].

Various factors contribute to shaping the bubble size distribution, encompassing operational parameters, liquid properties, and sparger configuration [6,7]. These factors collectively govern the dynamics of bubble formation and distribution.

Corresponding author: Liu LIU, Tel: +86-15111249166, E-mail: l.liu@csu.edu.cn
DOI: 10.1016/S1003-6326(24)66501-5

LAUPSIEN et al [8] examined the sensitivity of local bubble plume hydrodynamics to viscosity and sparger design. ZHANG et al [9] investigated the evolving characteristics of BSD during the transition from bubbly to slug flow by changing gas flow rates, thus illuminating the constraints of conventional distribution functions in describing this intricate transition. GUAN and YANG [10] identified a bimodal BSD distribution, a pattern that persists except at low superficial gas velocity of 0.01 m/s. The first peak becomes more evident by increasing 20% internals in the sparger, thus showcasing the direct influence of sparger design on bubble size distribution. KHANCHEZAR et al [11] discerned distinct thresholds of gas flow rates that dictate transitions between flow regimes for different nozzle sizes. In conclusion, gas flow rate and nozzle diameter significantly affect bubble size distribution, demanding more research for practical and scientific insights.

Apart from bubble size, the shape of bubbles influences the overall hydrodynamics of the system as well, since it is closely related to the drag force, lift force, bubble wake formation and path instability [12−15]. For simulations of gas−liquid two-phase flows in industrial equipment, precise simulation results will be obtained with an accurate representation of the initial bubble shape distribution that aligns with reality. Bubble shape is often quantified using the bubble aspect ratio (E), which represents the ratio of the minor axis (h) to the major axis (w) of the bubble along its orientation axes [16−18]. Recent research by LIU et al [17] has emphasized that the bubble aspect ratio is not solely determined by the bubble diameter but is substantially influenced by the nozzle diameter, indicating the sensitivity of bubble dynamics to the detachment process. Additionally, the gas flow rate represents another key parameter impacting bubble shape, as higher gas flow rates intensify bubble coalescence and breakup, further affecting the bubble aspect ratio. However, current knowledge of the bubble aspect ratio primarily relies on studies involving individual bubbles [19−21]. The investigation of bubble shape under swarm conditions, characterized by complex interactions among multiple bubbles, remains an essential research direction for further inquiry.

Various experimental techniques have been utilized for bubble size and shape measurement [22,23], with non-intrusive methods gaining attention for their capability to study flow conditions without disturbing the system dynamics [24]. In this work, the non-intrusive high-speed photography was used to experimentally explore the bubble dynamics in a bubble column, combined with an image processing algorithm for data analysis. The characteristics of bubble size and shape distributions under swarm conditions are thoroughly investigated across varying gas flow rates and nozzle diameters, enhancing understanding of the bubble behaviors.

2 Experimental

2.1 Bubble column

Bubble size and shape distributions are measured in a rectangular bubble column with dimensions of 0.25 m × 0.05 m × 1.5 m ($W \times D \times H_c$), as shown in Fig. 1. Choosing a thickness of 0.05 m for the bubble column was a practical compromise to facilitate high-speed photography and accurate bubble analysis. The bubble column is the same as the one used by LIU et al [25,26]. It is equipped with a two-hole sparger made of 10 mm-thick stainless steel, in which nozzles with diameters of 0.3, 0.6 or 2 mm are installed. The specific location of the two nozzles is well illustrated on the right side of Fig. 1. Air and deionized water were used as the gas and the liquid phase, respectively. The liquid height (H) was set to be 0.625 m. One of the measurement planes is located at a height of 312.5 mm (middle of the column), which is used for the measurements of the BSD, shape distributions and Sauter mean diameter. The motion of the bubble plumes in this region is considered to be stable. The other position is particularly located at the nozzle tip for the measurements of the bubble departure process. The bubbles in the bubble column were photographed by a high-speed camera (Q-VIT, AOS Technologies Co., Switzerland) with illumination from a 240 W LED-backlit light source. The sampling frequency of the high-speed camera is 250 fps and the image resolution is about 70 μm/px. The gas flow rate is controlled with a mass flow controller (FMA-A2300, Omega Co., USA), varying from 0.1 to 1.2 L/min. Notably, even at these relatively small

gas flow rates, the system demonstrates its capability to generate a wide range of bubble size distributions. During the experiment, the liquid temperature was maintained in the range of (25±0.5) °C. A total of 18 sets of experiments with different nozzle diameters, gas flow rates and Reynolds number through the hole were carried out, as shown in Table 1. Original bubble images at different gas flow rates are shown in Fig. 2. The high-speed photography measurement method can refer to the detailed description by LIU et al [26].

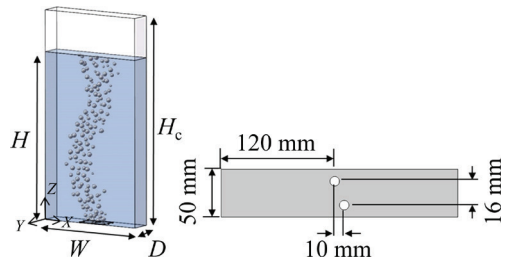

Fig. 1 Scheme of bubble column and ground plate [26]

Table 1 Combination of nozzle diameter and gas flow rate

No.	d_n/ mm	Q_g/ (L·min^{-1})	Re_{th}	No.	d_n/ mm	Q_g/ (L·min^{-1})	Re_{th}
1	0.3	0.1	511.0	10	0.6	0.6	1532.9
2	0.3	0.2	1021.9	11	0.6	0.8	2043.8
3	0.3	0.4	2043.8	12	0.6	1.2	3065.7
4	0.3	0.6	3065.7	13	2.0	0.1	76.6
5	0.3	0.8	4087.6	14	2.0	0.2	153.3
6	0.3	1.2	6131.5	15	2.0	0.4	306.6
7	0.6	0.1	255.5	16	2.0	0.6	459.9
8	0.6	0.2	511.0	17	2.0	0.8	613.1
9	0.6	0.4	1021.9	18	2.0	1.2	919.7

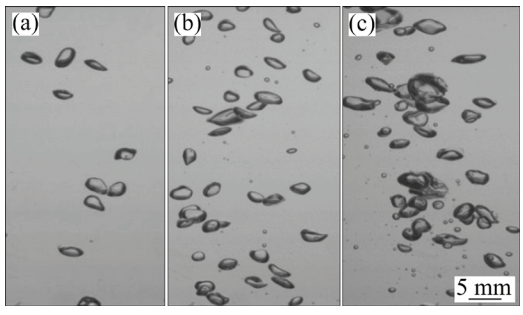

Fig. 2 Original bubble images at different gas flow rates with d_n=0.3 mm: (a) Q_g=0.1 L/min; (b) Q_g=0.4 L/min; (c) Q_g=0.8 L/min [26]

2.2 Digital image analysis

In order to obtain equivalent diameters and aspect ratios, a series of operations are performed upon the images. The outline of bubbles should be carefully captured as the gas flow rate increases and the overlap of bubbles occurs. The procedure of image processing and the calculation of bubble parameters by MATLAB software have been illustrated thoroughly by ZIEGENHEIN et al [27], ZIEGENHEIN and LUCAS [18] and LIU et al [26]. Under the assumption of oblate spheroids, the equivalent bubble diameter (d_{eq}, Eq. (1)) and the Sauter mean bubble diameter (d_{32}, Eq. (2)) are calculated based on the experimental data obtained by the image analysis. The bubble departure diameter ($d_{B,D}$ Eq. (3)) is calculated based on the detachment frequency during the bubble formation process.

$$d_{eq}=\sqrt[3]{w^2h} \tag{1}$$

$$d_{32}=\sum_i^N n_i d_{eq,i}^3 \Big/ \sum_i^N n_i d_{eq,i}^2 \tag{2}$$

$$d_{B,D}=10^{-4}\left(\frac{Q_g}{\pi f}\right)^{1/3} \tag{3}$$

Small bubbles retain a spherical or ellipsoidal shape, and the aspect ratio is defined and calculated by Eq. (4). However, bubbles deform considerably with the increase of the bubble diameter. In this situation, bubbles no longer maintain a spherical or ellipsoidal shape, but deform into an irregular shape. In this case, Fig. 3 shows a schematic diagram of an irregular deformed bubble, with the corresponding major axis (w) and minor axis (h) provided. The major axis is defined as the longest distance between two points of the projected bubble area, and the minor axis is the longest distance perpendicular to the major axis.

$$E=h/w \tag{4}$$

Error analysis is essential for the reliability of the bubble size and shape measurement in this study. To avoid repetition, a detailed discussion on the bubble detection procedure and data uncertainty can be found by LIU et al [26] based on the same experimental data, including the image number error, manual measurement error, and projection error. The statistical uncertainty of both bubble size and bubble aspect ratio were found to be below 3%.

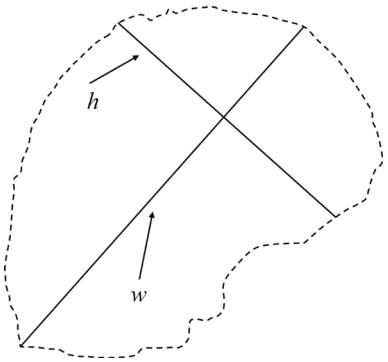

Fig. 3 Schematic diagram of bubble projection profile

3 Results and discussion

3.1 Bubble size distributions

3.1.1 Influence of gas flow rates and nozzle diameters

The BSD at different gas flow rates with nozzle diameters of 2, 0.6 and 0.3 mm is shown in Fig. 4. The probability density is calculated by dividing the number of bubbles in the interval by the total number of bubbles. Interestingly, the first peak occurs approximately at d_{eq}=1.5−2 mm for all gas flow rates and nozzle sizes with bimodal patterns. The consistent density peak distribution of 1.5−2 mm bubbles is influenced by the sub-bubble distribution during breakup, particularly under our specific experimental conditions. Remarkably, the same phenomenon is observed in the experimental results of LU et al [28]. This shared phenomenon could be attributed to the propensity of larger bubbles to fragment into smaller ones, with a notable preference for a diameter of 1.5−2 mm. Moreover, these small bubbles are relatively stable and exhibit a lower probability of coalescing to form larger bubbles. Changes in reactor or experimental conditions may affect breakup dynamics and sub-bubble distributions due to potential variations in reactor geometry and flow characteristics. The influence of experimental setups still needs further investigation.

For cases with a gas flow rate at 0.1 L/min in Figs. 4(a−c), the BSD shows unimodal behavior due to the limited occurrence of bubble coalescence and breakup effects at such low flow rates. As a result, there existed a notably narrow span of bubble diameters and a larger peak value. As the gas flow rate increases to 0.2 L/min, the BSD moves toward higher values due to the coalescence

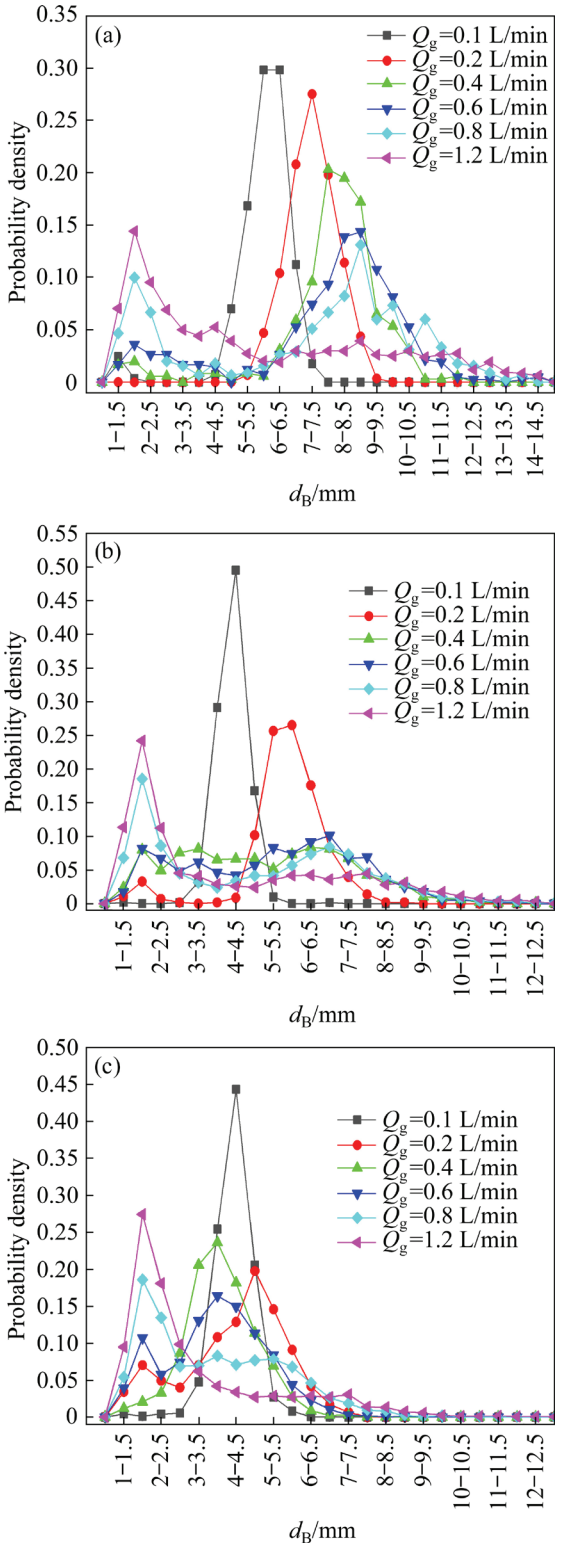

Fig. 4 Probability density distribution of bubble size (d_B) at different flow rates: (a) d_n=2 mm; (b) d_n=0.6 mm; (c) d_n=0.3 mm

of bubbles, which was also experimentally confirmed by BESAGNI and INZOLI [29]. The phenomenon of a transition from unimodal distribution to bimodal distribution agrees with the

studies concerning the size of the bubbles and the flow regime transition [30] and the findings of BESAGNI and INZOLI [31,32]. Similar bimodal distributions were also observed in other studies from the literature [33−36]. This might be attributed to the prevailing of bubble coalescence and breakup events with increasing the gas flow rates [34,36]. On the one hand, larger bubbles are formed owing to the bubble coalescence. On the other hand, the intensification of the bubble breakup results in much more small bubbles. It is worth noting that the BSD changes back to unimodal distribution in the small bubble region at Q_g=1.2 L/min. This indicates that, at high gas flow rates, the bubble breakup is intenser than that of coalescence and dominates the whole process. The phenomenon might be related to the enhancement of liquid turbulence intensity, but further investigation is needed.

In Fig. 4(b), the probability density of relatively large bubbles for the case with a nozzle of 0.6 mm is lower than that of the case with a larger nozzle of 2 mm except for Q_g=0.1 L/min, which is straightforward due to that the large bubbles are produced by large nozzles. In addition, it can be observed that the BSD is narrower with d_{eq} in the range of 1−8 mm. With a nozzle of 0.3 mm in Fig. 4(c), one difference is that the d_{eq} at the peak decreases with the gas flow rate increasing from 0.2 to 0.4 L/min, which indicates that the bubble breakup dominates the whole process and lots of small bubbles are produced in the column. As the nozzle diameter increases from 0.3 to 2 mm, the probability density of large bubbles increases for Q_g ranging from 0.2 to 1.2 L/min, while the probability density of small bubbles decreases. The peak that is located in the region of relatively large bubble sizes, shifts towards higher values with increasing nozzle diameter. At a gas flow rate of 0.1 L/min, a similar behavior is observed that the peak value shifts towards larger bubble diameters as the nozzle diameter increases.

3.1.2 Comparison with literature correlations

The Sauter mean diameter is widely used to characterize the bubble equivalent diameter in the field of multiphase flow. Figure 5 shows the calculated d_{32} with various nozzle diameters and gas flow rates. It can be observed that d_{32} increases with increasing the gas flow rate with nozzle sizes of 2 and 0.6 mm. However, in the case of 0.3 mm nozzle, d_{32} initially shows a slight decreasing trend, then increases as the gas flow rate increases from 0.05 to 1.2 L/min. According to the investigation by LIU et al [17], the smaller nozzle size causes bubbles to be more influenced by the nozzle under low to medium gas flow rates, leading to a higher likelihood of bubble breakup into smaller bubbles. This could explain why an inflection point occurs with a nozzle size of 0.3 mm.

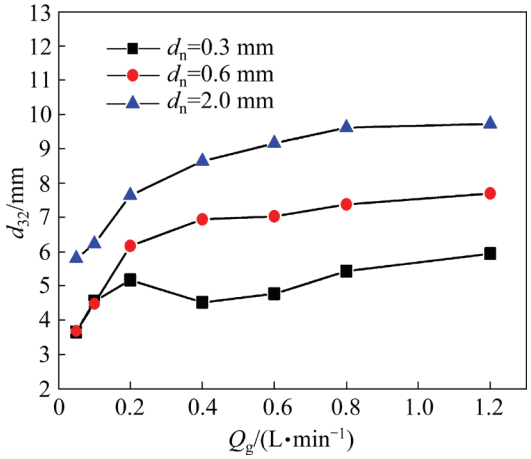

Fig. 5 Bubble Sauter mean diameter

In recent decades, different correlations relating the bubble diameter to the gas nozzle design parameters (i.e., gas flow rates and nozzle diameters) have been proposed. To assess the validity in relevant operating conditions, eight correlations (Eqs. (5)−(12)) are compared with the experimental observation.

The correlations proposed by POLLI et al [37] (Eq. (5)) and MIYAHARA et al [38] (Eq. (6)), which relate the dimensionless bubble diameter (d_w=$\langle d_{Exp}\rangle\{g\rho_L/(d_n\sigma)\}^{1/3}$) to the parameters of the system and the nozzle diameter d_n, are expressed by

$$d_w = 1.6722N_w^{0.333} \tag{5}$$

$$d_w = \begin{cases} 2.9, & N_w \le 1 \\ 2.9N_w^{-0.188}, & 1 < N_w \le 2 \\ 1.8N_w^{0.5}, & 2 < N_w \le 4 \\ 3.6, & N_w > 4 \end{cases} \tag{6}$$

The correlations proposed by DAVIDSON and AMICK [39] (Eq. (7)), KUMAR and KULOOR [40] (Eq. (8)), GADDIS and VOGELPOHL [41] (Eq. (9)), IGUCHI and CHIHARA [42] (Eqs. (10) and (11)) and JAMIALAHMADI et al [43] (Eq. (12)), which relate the bubble departure

diameter to the design parameters (the gas flow rate Q_g and the nozzle diameter d_n), are listed as follows:

$$d_{B,D}=0.54(Q_g d_n^{0.5})^{0.289} \tag{7}$$

$$d_{B,D}=\left(0.976\frac{Q_g^{1.2}}{g^{0.6}}\frac{6}{\pi}\right)^{1/3} \tag{8}$$

$$d_{B,D}=\left[\left(\frac{6d_n\sigma}{\rho_L g}\right)^{4/3}+\frac{81\mu_L Q_g}{\pi g}+\left(\frac{135Q_g^2}{4\pi^2 g}\right)^{4/5}\right]^{1/4} \tag{9}$$

$$d_{B,D}=\left(\frac{6Q_g}{1.06\pi}\right)^{1/3}\left(\frac{\sigma}{\rho_L g^3}\right)^{1/12}\left(\frac{\rho_L}{\rho_g}\right)^{1/15}\left[\frac{gd_n^5}{Q_g^2}\right]^{1/5} \tag{10}$$

$$d_{B,\,D\text{-Modified}}=1.25\left(\frac{6Q_g}{1.06\pi}\right)^{1/3}\left(\frac{\sigma}{\rho_L g^3}\right)^{1/12}\left(\frac{\rho_L}{\rho_g}\right)^{1/15}\left[\frac{gd_n^5}{Q_g^2}\right]^{1/5} \tag{11}$$

$$d_{B,D}=d_n\left[\frac{5}{Bd^{1.08}}+\frac{9.261Fr^{0.36}}{Ga^{0.39}}+2.147Fr^{0.51}\right]^{\frac{1}{3}} \tag{12}$$

Figure 6 shows the comparison of experimental data and the correlations [37,38] for the dimensionless velocity (N_w=$We/Fr^{1/2}$) and the dimensionless bubble diameter (d_w). For values of dimensionless velocity less than 12, the dimensionless bubble diameters are well estimated with the correlation of POLLI et al [37] For N_w>12, neither of the correlations can accurately reproduce the trend of d_w with increasing the dimensionless velocity.

In the following, the Sauter mean diameter is compared to the bubble departure diameter in order to investigate the evaluation of the bubble size. Figure 7 and Table 2 show corresponding values for both diameters as well as the bubble departure diameter predicted by various correlations [39−43] with a nozzle diameter of 2 mm. It can be seen from Fig. 7 that when the gas flow rate is in the range of 0.1−0.2 L/min, the values of d_{32} and the bubble departure diameter are nearly identical, indicating that the intensity of bubble coalescence and breakup is small. As the gas flow rate increases, intensified interactions between bubbles and the flow field lead to more pronounced coalescence and breakup. This dynamic interplay fundamentally alters the volumetric mean diameter d_{32} of the bubble population. When d_{32} is larger than the other, it means that more large bubbles are generated in the system due to coalescence, indicating a prevailing influence of coalescence over breakup processes in the system. The existing empirical correlations are not accurate enough to predict the change rule of the bubble departure diameter with the increase of flow rates. The correlation [42] slightly underestimates the bubble departure diameter at low gas flow rates and slightly overestimates it at high flow rates. Among them, the bubble departure diameter predicted by the correlation [43] is more consistent with the experimental results when the flow rate is in the range of 0.6−1.2 L/min. Table 2 shows that the correlation [42] exhibits the lowest mean relative error between the predicted values and the experimental data among all empirical correlations, which indicates that the correlation can better predict the variation of bubble departure diameter under the present experimental condition.

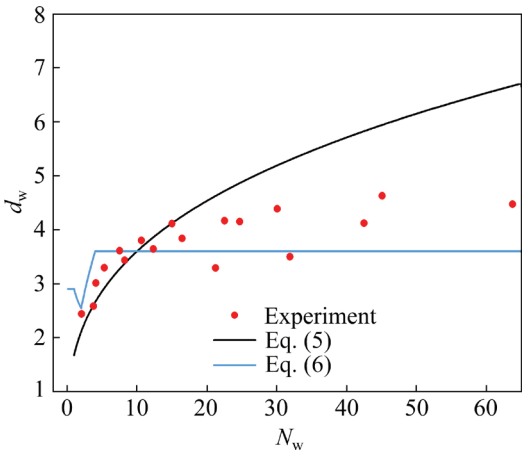

Fig. 6 Comparison with correlations of dimensionless velocity and dimensionless bubble diameter

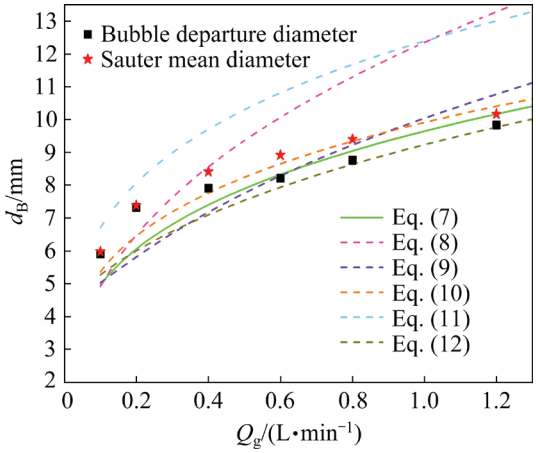

Fig. 7 Comparison of bubble departure diameter and Sauter mean diameter

Table 2 Comparison of experimental results and predicted bubble departure diameters

Source	Bubble departure diameter/mm						Mean relative error to departure diameter/%
	0.1 L/min	0.2 L/min	0.4 L/min	0.6 L/min	0.8 L/min	1.2 L/min	
Sauter mean diameter	5.98	7.38	8.41	8.92	9.4	10.17	−
Departure diameter	5.91	7.32	7.77	8.21	8.76	9.83	−
Eq. [7]	4.96	6.06	7.4	8.33	9.05	10.17	7.7
Eq. [8]	4.92	6.49	8.56	10.07	11.3	13.29	20.9
Eq. [9]	5.03	5.81	7.18	8.29	9.23	10.78	9.8
Eq. [10]	5.37	6.46	7.77	8.65	9.34	10.41	6.5
Eq. [11]	6.71	8.07	9.71	10.82	11.68	13.01	24.4
Eq. [12]	5.27	6	7.1	7.94	8.64	9.77	7.1%

3.2 Influence of gas flow rates on bubble aspect ratio distribution

Bubble deformation begins from the onset of bubble generation and is influenced not only by nozzle size and bubble size but also by local parameters such as gas volume fraction and turbulence. LIU et al [17] conducted an in-depth experimental study on the aspect ratio of single bubble rising in water and glycerol aqueous solution. Results show that the bubble shape changes from spherical to ellipsoidal, oblate ellipsoidal, skirted, and finally to strongly deformed shape as the bubble diameter increases. According to the relationship between bubble shape and aspect ratio, bubbles can be categorized roughly into spherical ($0.9<E<1$), ellipsoidal ($0.8<E<0.9$), oblate ellipsoidal ($0.6<E<0.8$), skirted ($0.3<E<0.6$) and strongly deformed shape ($E<0.3$). In addition, the comparison between experimental aspect ratios and predictions of empirical correlations can refer to the detailed discussion in the previous paper [26] based on the same experimental data.

In order to analyze the influence of gas flow rate on the bubble aspect ratio with different equivalent diameters, the bubbles are divided into 30 groups according to the diameter from 0 to 15 mm, and each group has a bubble diameter coverage of 0.5 mm. As shown in Fig. 8, the probability density distribution profile of the bubble aspect ratio for diameters ranging from 1 to 9 mm is provided. From Fig. 8(a), we can see that the probability density distributions of the aspect ratio of bubbles with a diameter of 1−2 mm are similar when the flow rate is 0.4−1.2 L/min, only a bias toward the smaller value side at 0.2 L/min. This suggests that the influence of gas flow rate on the bubble shape is less pronounced for diameters between 1 and 2 mm. For bubbles with a diameter of 2−3 mm, the aspect ratio distribution tends to the larger value side, as shown in Fig. 8(b). For bubbles with a diameter of 3−7 mm, results show that the aspect ratio probability density distribution of the case with a gas flow rate of 1.2 L/min tends to the side with a larger aspect ratio compared to other gas flow rates. For other gas flow rates, the peaks of aspect ratio probability distributions are all located around E of 0.5, which is in consistent with the conclusion in the previous study that the bubble aspect ratio tends to be a constant value with increasing the bubble diameter [26].

4 Conclusions

(1) When the gas flow rate increases from 0.1 to 0.2 L/min, the d_B corresponding to the peak probability density increases as well, demonstrating the preponderance of bubble coalescence. As the gas flow rate continues to increase to 1.2 L/min, the peak shifts to smaller d_B, and the bubble breakup is dominant.

(2) With the increase of gas flow rate, a change of BSD from unimodal to bimodal is found under all nozzles. In bimodal distribution, one peak is located in the small bubble diameter of 1.5−2 mm and the other is located in the relatively large bubble diameter. As the nozzle diameter increases, the probability density of large bubbles increases as well except for Q_g=0.1 L/min.

(3) Under the condition with a nozzle diameter of 2 mm, the Sauter mean diameters of bubbles are

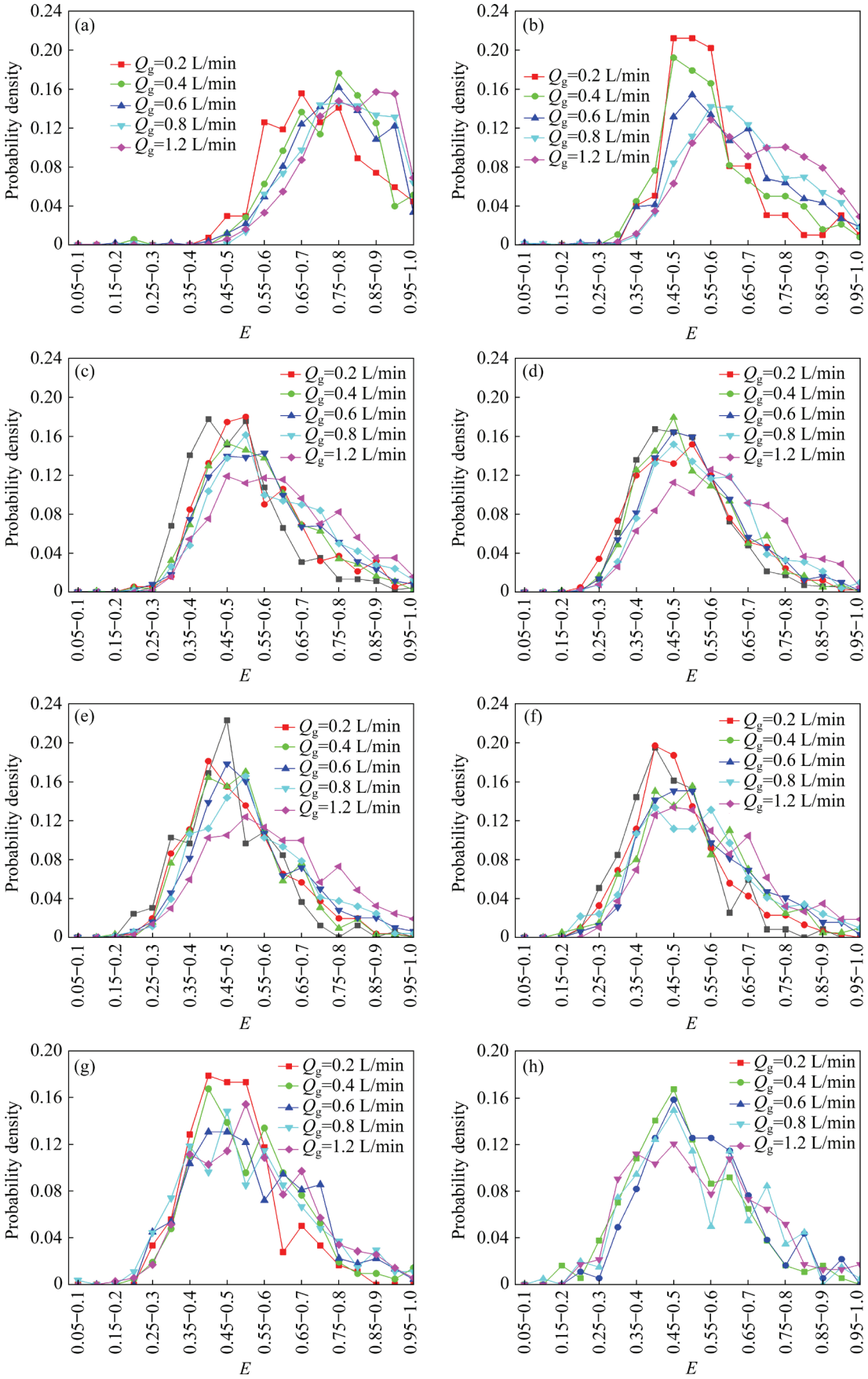

Fig. 8 Influence of gas flow rate on probability density distribution of bubble aspect ratio under different bubble diameters: (a) 1−2 mm; (b) 2−3 mm; (c) 3−4 mm; (d) 4−5 mm; (e) 5−6 mm; (f) 6−7 mm; (g) 7−8 mm; (h) 8−9 mm

larger than the bubble departure diameters in the range of 0.1−1.2 L/min. On average, the bubble coalescence is stronger than the breakup. Among all the correlations, the Iguchi and Chihara model can better predict the variation of bubble departure diameter with increasing the gas flow rates.

(4) The bubble shape is less affected by the gas flow rate for bubbles within 1−2 mm. When the bubble diameter is 3−9 mm, the peak of bubble aspect ratio probability distribution is mostly near E=0.5 as the gas flow rate increases.

Nomenclature

$Bd=\frac{\rho_L g d_n^2}{\sigma}$	Bond number
D/m	Depth of bubble column
d_{32}/mm	Sauter mean bubble diameter
d_B/mm	Diameter of bubble
$d_{B,D}$/mm	Bubble departure diameter
d_{eq}/mm	Bubble equivalent diameter
d_{EXP}/mm	Experimental mean diameter of bubble
d_n/mm	Nozzle diameter
d_w	Dimensionless mean diameter
E	Aspect ratio
f/s^{-1}	Bubble formation frequency
$Fr=\frac{U_{th}^2}{g d_n}$	Froude number
g/(m·s^{-2})	Gravitational acceleration
$Ga=\frac{\rho_L^2 d_n^3 g}{\mu_L^2}$	Galileo number
h/mm	Bubble minor axis
H_c/m	Height of bubble column
N_w	Dimensionless velocity
Q_g/(L·min^{-1})	Gas flow rate
$Re_{th}=\frac{\rho_g U_{th} d_n}{\mu_g}$	Reynolds number through the hole
U_{th}/(m·s^{-1})	Gas velocity through the hole
w/mm	Bubble major axis
W/m	Width of bubble column
$We=\frac{\rho_L U_{th}^2 d_n}{\sigma}$	Weber number
μ_L/(Pa·s)	Liquid viscosity
μ_g/(Pa·s)	Gas viscosity
ρ_L/(kg·m^{-3})	Liquid density
ρ_g/(kg·m^{-3})	Gas density
σ/(N·m^{-1})	Surface tension

CRediT authorship contribution statement

Hong-jie YAN: Supervision, Writing − Reviewing and editing; **He-yang ZHANG:** Writing and editing; **Liu LIU:** Methodology, Experiment and writing; **Thomas ZIEGENHEIN:** Experiment and editing; **Ping ZHOU:** Writing − Reviewing and editing.

Declaration of competing interest

The authors declare that they have no known competing financial interests or personal relationships that could have appeared to influence the work reported in this paper.

Acknowledgments

This work was supported by the National Natural Science Foundation of China (No. 51906262), the Natural Science Foundation of Hunan Province, China (No. 2020JJ5735), and the Youth Excellent Sci−Tech Talents Training Plan under Hunan Provincial Sci−Tech Talents Sponsorship Program, China (No. 2023TJ-N10).

References

[1] YAN Hong-jie, XIAO Jun-bing, SONG Yan-po, HU Zhi-wen, TAN Zhi-kai, LIU Liu. Cold model on bubble growth and detachment in bottom blowing process [J]. Transactions of Nonferrous Metals Society of China, 2019, 29(1): 213−221.

[2] CHEN Zhi-bin, YAN Hong-jie, ZHOU Ping, YANG Ping, DING Jie-hui, LIU Jia, LIU Liu. Parametric study of gas−liquid two-phase flow field in horizontal stirred tank [J]. Transactions of Nonferrous Metals Society of China, 2021, 31(6): 1806−1817.

[3] LIU Liu, CHEN Zhi-bin, YAN Hong-jie, ZHANG Deng-kai, ZHOU Ping. Numerical simulation and multi-objective parameter optimization of gas−liquid flow in horizontal stirred tank [J]. Transactions of Nonferrous Metals Society of China, 2023, 33(3): 958−968.

[4] SCHÄFER R, MERTEN C, EIGENBERGER G. Bubble size distributions in a bubble column reactor under industrial conditions [J]. Experimental Thermal and Fluid Science, 2002, 26(6/7): 595−604.

[5] RAMKRISHNA D, SINGH M R. Population balance modeling: Current status and future prospects [J]. Annual Review of Chemical and Biomolecular Engineering, 2014, 5: 123−146.

[6] PRAKASH R, KUMAR MAJUMDER S, SINGH A. Bubble size distribution and specific bubble interfacial area in two–

phase microstructured dense bubbling bed [J]. Chemical Engineering Research and Design, 2020, 156, 108−130.

[7] BESAGNI G, INZOLI F, ZIEGENHEIN T. Two-phase bubble columns: A comprehensive review [J]. ChemEngineering, 2018, 2(2): 13.

[8] LAUPSIEN D, LE MEN C, COCKX A, LINÉ A. Effects of liquid viscosity and bubble size distribution on bubble plume hydrodynamics [J]. Chemical Engineering Research and Design, 2021, 180: 451−469.

[9] ZHANG M H, WANG G Y, PAN L M, ISHII M. Experimental study of bubble size distribution in bubbly and bubbly-to-slug transition flow [J]. International Journal of Multiphase Flow, 2022, 146: 103852.

[10] GUAN X P, YANG N. Bubble size distribution in a bubble column with vertical tube internals: Experiments and CFD-PBM simulations [J]. AIChE Journal, 2022, 68(9): 17755.

[11] KHANCHEZAR S, HASHEMI-NAJAFABADI S, SHOJAOSADATI S A, BABAEIPOUR V. Hydrodynamics and mass transfer in miniaturized bubble column bioreactors [J]. Bioprocess and Biosystems Engineering, 2019, 42, 257−266.

[12] KONG G, MIRSANDI H, BUIST K A, PETERS E A J F, BALTUSSEN M W, KUIPERS J A M. Hydrodynamic interaction of bubbles rising side-by-side in viscous liquids [J]. Experiments in Fluids, 2019, 60(10): 155.

[13] XU Xiao-fei, ZHANG Ju, LIU Feng-xia, WANG Xiao-juan, WEI Wei, LIU Zhi-jun. Rising behavior of single bubble in infinite stagnant non-Newtonian liquids [J]. International Journal of Multiphase Flow, 2017, 95: 84−90.

[14] PANG Ming-jun, WEI Jin-jia. Analysis of drag and lift coefficient expressions of bubbly flow system for low to medium Reynolds number [J]. Nuclear Engineering and Design, 2011, 241(6): 2204−2213.

[15] HESSENKEMPER H, ZIEGENHEIN T, RZEHAK R, LUCAS D, TOMIYAMA A. Lift force coefficient of ellipsoidal single bubbles in water [J]. International Journal of Multiphase Flow, 2021, 138: 103587.

[16] ELLINGSEN K, RISSO F. On the rise of an ellipsoidal bubble in water: Oscillatory paths and liquid-induced velocity [J]. Journal of Fluid Mechanics, 2001, 440: 235−268.

[17] LIU Liu, YAN Hong-jie, ZHAO Guo-jian. Experimental studies on the shape and motion of air bubbles in viscous liquids [J]. Experimental Thermal and Fluid Science, 2015, 62: 109−121.

[18] ZIEGENHEIN T, LUCAS D. Observations on bubble shapes in bubble columns under different flow conditions [J]. Experimental Thermal and Fluid Science, 2017, 85: 248−256.

[19] DUINEVELD P C. The rise velocity and shape of bubbles in pure water at high Reynolds number [J]. Journal of Fluid Mechanics, 1995, 292: 325−332.

[20] SANADA T, SUGIHARA K, SHIROTA M, WATANABE M. Motion and drag of a single bubble in super-purified water [J]. Fluid Dynamics Research, 2008, 40(7/8): 534−545.

[21] SATO A, SHIROTA M, SANADA T, WATANABE M. Shape and steady drag on single rising bubbles [J]. Progress in Multiphase Flow Research, 2008, 3: 35−41.

[22] MESA D, BRITO-PARADA P R. Bubble size distribution in aerated stirred tanks: Quantifying the effect of impeller-stator design [J]. Chemical Engineering Research and Design, 2020, 160: 356−369.

[23] LEONARD C, FERRASSE J H, LEFEVRE S, VIAND A, BOUTIN O. Bubble rising velocity and bubble size distribution in columns at high pressure and temperature: From lab scale experiments to design parameters [J]. Chemical Engineering Research and Design, 2021, 173: 108−118.

[24] ZARUBA A, KREPPER E, PRASSER H M, SCHLEICHER E. Measurement of bubble velocity profiles and turbulent diffusion coefficients of the gaseous phase in rectangular bubble column using image processing [J]. Experimental Thermal and Fluid Science, 2005, 29(7): 851−860.

[25] LIU Liu, YAN Hong-jie, ZIEGENHEIN T, HESSENKEMPER H, LI Qing, LUCAS D. A systematic experimental study and dimensionless analysis of bubble plume oscillations in rectangular bubble columns [J]. Chemical Engineering Journal, 2019, 372: 352−362.

[26] LIU Liu, ZHANG He-yang, YAN Hong-jie, ZIEGENHEIN T, HESSENKEMPER H, ZHOU Ping, LUCAS D. Experimental studies on bubble aspect ratio and corresponding correlations under bubble swarm condition [J]. Chemical Engineering Science, 2021, 236: 116551.

[27] ZIEGENHEIN T, ZALUCKY J, RZEHAK R, LUCAS D. On the hydrodynamics of airlift reactors. Part I: Experiments [J]. Chemical Engineering Science, 2016, 150: 54−65.

[28] LU Xia, DING Yi-gang, YU Jiu-yang, LONG Bing-wen, ZHENG Xiao-tao. Experimental study of hydrodynamics and bubble size distribution of an external loop airlift reactor [J]. The Canadian Journal of Chemical Engineering, 2019, 97(Suppl.): 1685−1693.

[29] BESAGNI G, INZOLI F. Bubble sizes and shapes in a counter-current bubble column with pure and binary liquid phases [J]. Flow Measurement and Instrumentation, 2019, 67: 55−82.

[30] LUCAS D, KREPPER E, PRASSER H M. Evolution of flow patterns, gas fraction profiles and bubble size distributions in gas-liquid flows in vertical tubes [J]. Transactions of the Institute of Fluid-Flow Machinery, 2003, 112: 37−46.

[31] BESAGNI G, INZOLI F. Bubble size distributions and shapes in annular gap bubble column [J]. Experimental Thermal and Fluid Science, 2016, 74: 27−48.

[32] BESAGNI G, INZOLI F. Comprehensive experimental investigation of counter-current bubble column hydrodynamics: Holdup, flow regime transition, bubble size distributions and local flow properties [J]. Chemical Engineering Science, 2016, 146: 259−290.

[33] HERNANDEZ-AGUILAR J R, COLEMAN R G, GOMEZ C O, FINCH J A. A comparison between capillary and imaging techniques for sizing bubbles in flotation systems [J]. Minerals Engineering, 2004, 17(1): 53−61.

[34] LAU Y M, SUJATHA K T, GAEINI M, DEEN N G, KUIPERS J A M. Experimental study of the bubble size distribution in a pseudo-2D bubble column [J]. Chemical Engineering Science, 2013, 98: 203−211.

[35] PARTHASARATHY R, AHMED N. Bubble size

distribution in a gas sparged vessel agitated by a Rushton turbine [J]. Industrial & Engineering Chemistry Research, 1994, 33(3): 703−711.
[36] WONGSUCHOTO P, CHARINPANITKUL T, PAVASANT P. Bubble size distribution and gas–liquid mass transfer in airlift contactors [J]. Chemical Engineering Journal, 2003, 92(1/2/3): 81−90.
[37] POLLI M, DI STANISLAO M, BAGATIN R, BAKR E A, MASI M. Bubble size distribution in the sparger region of bubble columns [J]. Chemical Engineering Science, 2002, 57(1): 197−205.
[38] MIYAHARA T, MATSUBA Y, TAKAHASHI T. Size of bubbles generated from perforated plates [J]. International Journal of Chemical Engineering, 1982, 8(1): 13−17. (in German)
[39] DAVIDSON L, AMICK E H. Formation of gas bubbles at horizontal orifices [J]. AIChE Journal, 1956, 2(3): 337−342.
[40] KUMAR R, KULOOR N K. The formation of bubbles and drops [J]. Advances in Chemical Engineering, 1970, 8(8): 253−368.
[41] GADDIS E S, VOGELPOHL A. Bubble formation in quiescent liquids under constant flow conditions [J]. Chemical Engineering Science, 1986, 41(1): 97−105.
[42] IGUCHI M, CHIHARA T. Water model study of the frequency of bubble formation under reduced and elevated pressures [J]. Metallurgical and Materials Transactions B, 1998, 29(4): 753−761.
[43] JAMIALAHMADI M, ZEHTABAN M R, MÜLLER-STEINHAGEN H, SARRAFI A, SMITH J M. Study of bubble formation under constant flow conditions [J]. Chemical Engineering Research and Design, 2001, 79(5): 523−532.

气体流量和喷嘴直径对鼓泡塔内气泡大小和形状分布的影响

闫红杰[1]，张河杨[1]，刘 柳[1]，Thomas ZIEGENHEIN[2]，周 萍[1]

1. 中南大学 能源科学与工程学院，长沙 410083；
2. TIV Consultancy, 7th Pl Road 1312, 85281 Tempe, Arizona, United States

摘 要：通过高速摄影结合图像处理算法，研究气体流量和喷嘴直径对气泡尺寸和纵横比分布的影响。结果表明，在所有喷嘴直径下，气泡当量直径的概率密度呈现双峰分布，其中第一个峰值接近直径为 1.5~2 mm 的小气泡区域，另一个峰值位于较大的气泡区域。将气体流量从 0.1 L/min 增加到 0.2 L/min 会导致大气泡的概率密度更高，表明气泡聚并现象普遍存在。当气体流量增加至 1.2 L/min 时，峰值对应的气泡直径变小，并且气泡破裂占主导地位。对于直径为 1~2 mm 的气泡，形状受气体流量的影响较小，而 3~9 mm 的气泡在所有气体流量下气泡纵横比概率密度分布的峰值均位于纵横比 $E = 0.5$ 处。Iguchi 和 Chihara 提出的模型能更好地预测气泡脱离直径随气体流量的增大的变化。

关键词：气泡尺寸分布；气泡直径；气泡纵横比；气体流量；喷嘴直径；鼓泡塔

(Edited by Xiang-qun LI)